





## Article

# Image Quality and Information Parameters of Electronic Portal Imaging Devices

Marios K. Tzomakas <sup>1</sup>, Vasiliki Peppas <sup>2</sup> , Antigoni Alexiou <sup>2</sup>, Georgios Karakatsanis <sup>2</sup>, Anastasios Episkopakis <sup>3,4</sup>, Christos Michail <sup>1</sup> , Ioannis Valais <sup>1</sup> , George Fountos <sup>1</sup>, Nektarios Kalyvas <sup>1,\*</sup>  and Ioannis S. Kandarakis <sup>1</sup>

<sup>1</sup> Radiation Physics, Materials Technology and Biomedical Imaging Laboratory, Department of Biomedical Engineering, University of West Attica, 12210 Athens, Greece; mtzomakas@uniwa.gr (M.K.T.); cmichail@uniwa.gr (C.M.); valais@uniwa.gr (I.V.); gfoun@uniwa.gr (G.F.); kandarakis@uniwa.gr (I.S.K.)

<sup>2</sup> Department of Radiotherapy, General Hospital of Athens Alexandra, 11528 Athens, Greece; vpeppas@med.uoa.gr (V.P.); antalexio@hotmail.com (A.A.); gekarakatsanis@gmail.com (G.K.)

<sup>3</sup> Elekta, 15124 Athens, Greece; aepiskopakis@med.uoa.gr

<sup>4</sup> Medical Physics Laboratory, Medical School, National and Kapodistrian University of Athens, 11527 Athens, Greece

\* Correspondence: nkalyvas@uniwa.gr

**Abstract:** In this study, the imaging performance of electronic portal imaging devices (EPIDs) is evaluated, comparing measurements collected from EPID images captured at 115 cm, with a field size of  $15 \times 15 \text{ cm}^2$ , monitor units (MUs) in the range of 2 MU–100 MU and dose rates (DRs) of 200 MU/min, 400 MU/min and 600 MU/min, using a 6 MV LINAC system and the QC-3V image quality phantom. The analysis includes the normalized contrast transfer function (CTF<sub>norm</sub>), the noise power spectrum (NPS) and the information capacity (IC), as well as the signal-to-noise frequency response (SNFR), which can be used as a comprehensive quality index. The results of our study are compared with previously published data captured at 100 cm under similar exposure conditions. They show similar CTF curves with different source-to-phantom distances, with the lowest values observed at specific MU and DR combinations. Moreover, NPS graphs are found to decrease with respect to spatial frequency. SNFR values also display a reduction with increasing spatial frequency. In addition, irradiation with the phantom placed closer to the EPID, 115 cm from the LINAC, yields better SNFR and IC performance characteristics, indicating better delineation of the organs closer to the EPID. The testing of EPID performance may potentially benefit from our results, which may lead to improvements in the quality of radiotherapy treatments.

**Keywords:** EPID; LINAC; image quality information; MTF; performance quality index metrics; QC-3V



**Citation:** Tzomakas, M.K.; Peppas, V.; Alexiou, A.; Karakatsanis, G.; Episkopakis, A.; Michail, C.; Valais, I.; Fountos, G.; Kalyvas, N.; Kandarakis, I.S. Image Quality and Information Parameters of Electronic Portal Imaging Devices. *Appl. Sci.* **2024**, *14*, 10260. <https://doi.org/10.3390/app142210260>

Academic Editor: Pedro Couto

Received: 7 October 2024

Revised: 1 November 2024

Accepted: 5 November 2024

Published: 7 November 2024



**Copyright:** © 2024 by the authors. Licensee MDPI, Basel, Switzerland. This article is an open access article distributed under the terms and conditions of the Creative Commons Attribution (CC BY) license (<https://creativecommons.org/licenses/by/4.0/>).

## 1. Introduction

Electronic portal imaging devices (EPIDs) play a crucial role in modern radiotherapy, offering precise imaging capabilities, essential for both patient positioning verification and quality assurance (QA) of linear accelerators (LINACs) [1]. Over time, their functionality has been extended beyond geometric accuracy validation to include dosimetric data acquisition and treatment verification, particularly in the context of advanced radiotherapy techniques, like intensity-modulated radiation therapy (IMRT) and volumetric-modulated arc therapy (VMAT) [2].

In the sector of EPID QA, the evaluation of imaging performance is crucial to ensure the reliability and accuracy of acquired images [3–6]. Current EPID quality control protocols measure image spatial resolution through phantom visualization or in terms of spatial frequency [1,2,4–6]. In addition, uniformity, contrast and noise measurements have also been considered [2,3]. A prerequisite in image quality is the use of holistic parameters

which can provide information about the signal and noise in the spatial frequency domain. Such a parameter is the detective quantum efficiency (DQE), whose calculation requires the MTF as well as the calculation of noise in the spatial frequency domain. The DQE calculation has been reported in the current literature [1,4,6–8]. These calculations, however, require data about X-ray fluence which are either difficult to obtain through measurements or are tabulated [1,4,6–8] and thus may not be case-specific.

Among the array of metrics used for this purpose, the signal-to-noise frequency response (SNFR) has recently [3] appeared as a universal indicator of EPID image quality. SNFR determination requires the calculation of the contrast transfer function (CTF) and the noise power spectrum (NPS) [3]. It can be considered a substitute for detective quantum efficiency (DQE), which is often applied in X-ray medical imaging [1]. A drawback of the aforementioned methodology is the need for a bar pattern phantom for the calculation of the CTF. However, this requirement can be easily offset in SNFR calculations by the availability of specific phantoms. Previously published work [3] has studied variations in the SNFR in terms of dose rate (DR) and monitor unit (MU) choice with an experimental setup, incorporating a QC-3V imaging performance phantom placed 100 cm from the source and the head of the LINAC. It was found that in clinical imaging settings, the image algorithms imposed by iViewGT™ version R3.4.1 b519 software of the EPID affects the final image quality metrics [1,4–6].

This work focuses on examining whether other holistic imaging performance metrics that can be calculated in clinical imaging radiotherapy conditions can provide useful data. Such a parameter is information capacity (IC), giving the available information in bits/mm<sup>2</sup> [9,10]. Information capacity has been investigated within the framework of Shannon's information theory to quantify the information signal that is transmitted through an electronic communication channel without errors [11]. The concept of information capacity has been previously used effectively as an imaging performance metric in diagnostic radiology and in nuclear medicine [12]. To our knowledge, it has not been previously used in portal imaging of radiation therapy. The calculation of this parameter includes NPS measurements and modulation transfer function (MTF) calculations; thus, it can be regarded as a prominent candidate for comparison with the SNFR [3]. In addition, a comparison of SNFR and IC usability is attempted.

Furthermore, it might be of clinical use to determine the effect of patient positioning distance during EPID imaging. Thus, in this work, the SNFR and IC were studied at two phantom distances from the LINAC head at 100 cm and 115 cm, that is closer to the detector. This distance difference incorporates body shape sizes and may provide a deeper understanding of the effect of scatter and imaging geometry on EPID imaging. The results of this investigation may assist in the development of optimized QA protocols for LINACs in radiotherapy settings and may contribute to a better evaluation of patient positioning images.

## 2. Materials and Methods

The study aimed to systematically evaluate the imaging performance of an electronic portal imaging device (EPID), applying the SNFR and IC of an EPID used in the Infinity™ LINAC manufactured by Elekta AB, Stockholm, Sweden, under literature-based irradiation conditions [3]. Available SNFR published data for a QC-3V phantom at a distance of 100 cm were used and compared with IC values that have been calculated in this work. In addition, a new experimental setup where the source-to-phantom distance was set at 115 cm was employed in order to examine the effect of changes in image geometry compared to a previous work with irradiation at 100 cm [3]. The imaging performance evaluation at different source-to-phantom distances can simulate varying treatment scenarios encountered in clinical practice. Alongside the SNFR and IC, other parameters like the signal-to-noise-ratio (SNR) have been calculated. The QC-3V phantom, a standard tool for EPID image quality evaluation, was used in this study [3]. DICOM RT format images with a pixel size of  $0.40 \times 0.40$  mm<sup>2</sup> were acquired as previously described [3], while image analysis was

conducted using ImageJ version 1.52a and custom MATLAB version R2021b software. The following methods and formulas were used to determine the image quality and system performance metrics. The exposure conditions were from 2 MU to 100 MU so as to not only examine typical EPID imaging under low MU values, but also investigate the response of EPID in conditions closer to treatment settings. In addition, the chosen dose rates (DRs) were 200 MU/min, 400 MU/min and a LINAC maximum dose rate (DR) of 600 MU/min so as to check the fast dose delivery treatment conditions.

The CTF was used as an index for determining the response of spatial frequency,  $f$ , as follows [4,7,8,12–17]:

$$\text{MTF}(f) = \frac{\pi}{4} \left[ \text{CTF}(f) + \frac{\text{CTF}(3f)}{3} - \frac{\text{CTF}(5f)}{5} + \dots \right] \quad (1)$$

$$\text{CTF}(f) = \frac{\mu_{\max}(f) - \mu_{\min}(f)}{\mu_{\max}(f) + \mu_{\min}(f)} \quad (2)$$

where the local maximum pixel value is  $\mu_{\max}(f)$ , and the local minimum pixel value is  $\mu_{\min}(f)$ , for a given frequency  $f$ , corresponding to five regions of the phantom [18]. The contrast transfer function (CTF) was computed for each corresponding set of line pairs located in the QC-3V phantom for each frequency [10,14,15].

The CTF and MTF describe the resolution in the spatial frequency domain. High values of these parameters at each spatial frequency indicate the ability of the EPID to image small objects. Checking these parameters during an EPID QC determines how well the EPID can delineate an organ or image a small-sized area [19,20].

The SNR was calculated using mean pixel values and standard deviations of regions of interest (ROIs), allowing for the estimation of a signal within a noisy background [21].

$$\text{SNR} = \frac{\mu_{\text{ROI}}}{\sigma} \quad (3)$$

where  $\mu_{\text{ROI}}$  represents the mean pixel value of the region of interest (ROI) and  $\sigma$  denotes the standard deviation associated with that ROI. The SNR is used to estimate the signal present within the noise. The SNR provides a means for characterizing image clarity. High-SNR EPID images effectively assert the accuracy of patient positioning.

The NPS was utilized to analyze noise characteristics in the spatial frequency domain [10,22]. The ROI used was in air.

$$\text{NPS}(f_x, f_y) = \frac{\left\langle \left| \text{FFT} \left( \sum_{n_x=0}^{N_x-1} \sum_{n_y=0}^{N_y-1} p(x, y) \right) \right|^2 \right\rangle}{N_x N_y \Delta x \Delta y} \quad (4)$$

The NPS is a measure of the noise distribution in the spatial frequency domain, giving a limit of image clarity, especially in small contrast tissues.

The SNFR can be derived straightforwardly from the CTF and NPS and operates as a comprehensive image quality index associated with the signal-to-noise ratio in the spatial frequency domain [3].

$$\text{SNFR}(f) = \frac{(\mu_{\text{CTF}_{\text{norm}}}(f))^2}{\text{NPS}(f)} \quad (5)$$

According to Shannon's theory, the image IC was calculated using the MTF and the NPS [9,10].

$$\text{IC} = \pi \int_0^{\infty} \log_2 \left\{ 1 + \frac{[\mu \cdot \text{MTF}(f)]^2}{\text{NPS}(f)} \right\} f df \quad (6)$$

The SNFR and IC are holistic parameters calculated by means of the MTF, CTF and NPS. They both provide information about the SNR in the spatial frequency domain, thus enabling the determination of the imaging capabilities of the EPID.

The phantom used in this work does not incorporate enough spatial frequencies to accurately calculate the MTF of the system. A method proposed in the literature [3] has been used where the CTF values, calculated by Equation (2), were extrapolated at higher spatial frequencies. This method allowed for an approximation of the MTF by using Equation (1), hereafter referred to as the aMTF [3] and the subsequent calculation of the IC.

In general, these methods permit a comparative evaluation of EPID imaging performance under different source-to-phantom distances, while maintaining the stability of MUs and DRs, thus providing important information about system functionality and image quality in order to benefit different radiotherapy treatments.

### 3. Results

In Figure 1, the aMTF curves for source–phantom distances of 100 cm [3] and 115 cm, using 2 MUs at a 200 DR, a 400 DR and a 600 DR are demonstrated. The aMTF curves were approximated through the CTF using a method described in the literature [3]. The aMTF values from 0.1 lp/mm to 0.212 lp/mm are nearly identical, differing by only 0–2.37%. From 0.212 lp/mm to 0.789 lp/mm, the aMTF values for the 100 cm distance are lower than those for the 115 cm distance. Specifically, at 0.463 lp/mm, there is a difference of 10.84%, and at 0.789 lp/mm, a 10.20% increase is observed for the 115 cm distance. The lower values at 100 cm might indicate an increase in the X-ray spread due to the incident scattered X-rays on the detector (i.e., larger air gap). In the energy range applied in radiation therapy, X-ray scatter occurs at small scattering angles, i.e., mainly in forward directions. However, the proximity of the phantom to the EPID, under 115 cm irradiation conditions, results in a reduced spread of the scatter X-rays, i.e., scattered X-rays are distributed in a smaller area on the detector’s entrance surface than in the case at 100 cm. This is manifested in a seemingly higher MTF.

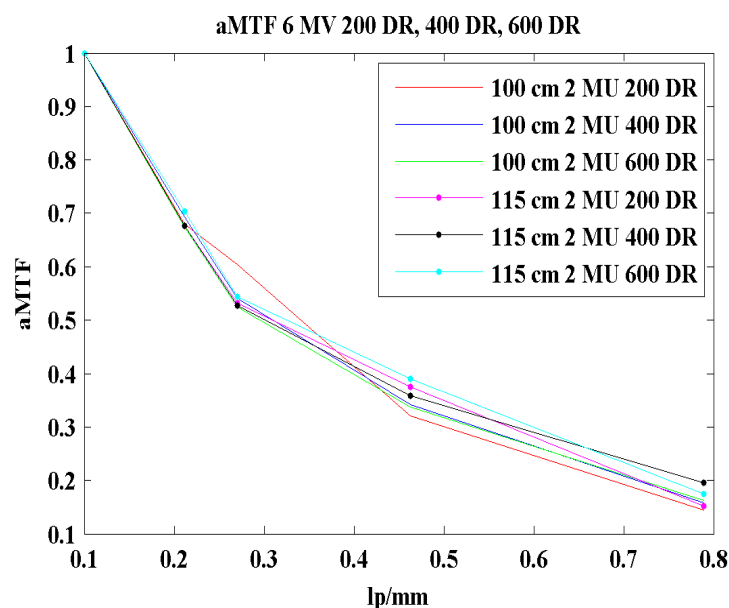


**Figure 1.** aMTF graphs of 100 cm using 2 MUs and 115 cm using 2 MUs with 200 DR, 400 DR and 600 DR (1 DR = 1 MU/min).

In Figure 2, the aMTF graphs for 100 cm and 115 cm source–phantom distances using 100 MUs at a 200 DR, a 400 DR and a 600 DR are shown. Similar to Figure 1, the aMTF values from 0.1 lp/mm to 0.212 lp/mm are almost equal, with only a 0–1% difference. From 0.212 lp/mm to 0.789 lp/mm, the aMTF values for the 100 cm distance are lower than those for the 115 cm distance. At 0.463 lp/mm, the difference is 10.10%, and at 0.789 lp/mm, it is approximately 18.13% for the 115 cm distance. The persistent degradation of the aMTF values for the 100 cm distance, for higher MUs, may suggest that this behavior is

more affected by X-ray physics than the software manipulation imposed in clinical EPID imaging [3,23].

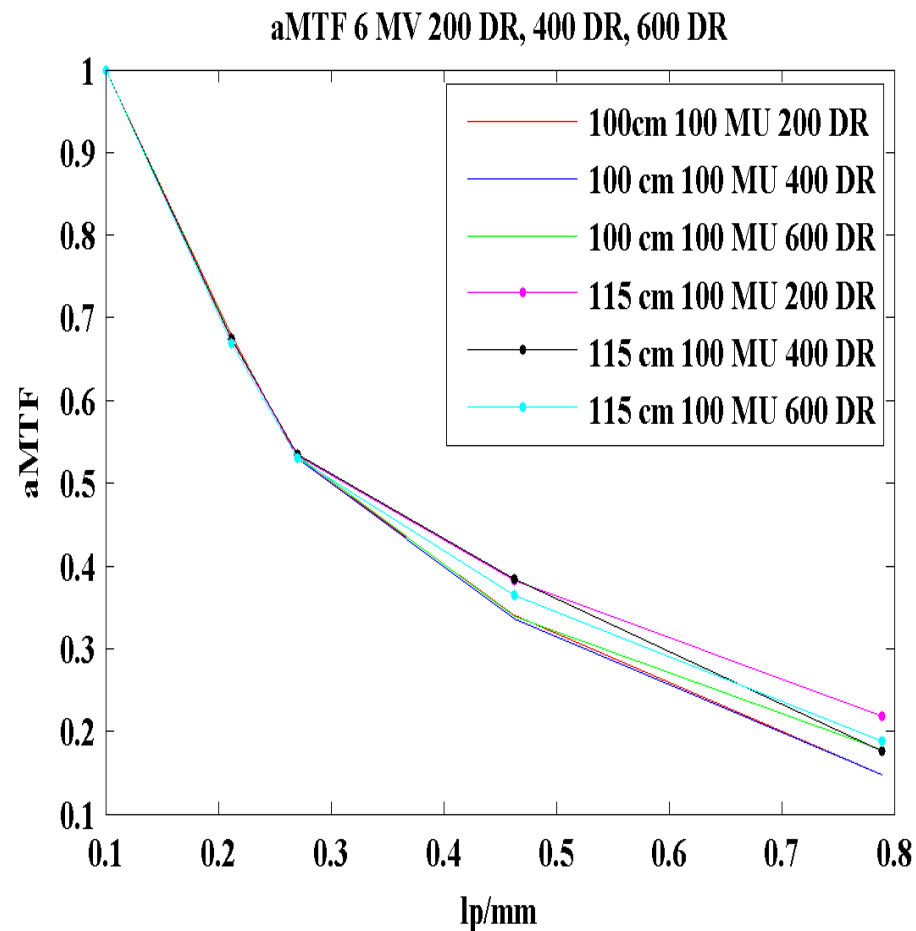


**Figure 2.** aMTF graphs of 100 cm using 100 MUs and 115 cm using 100 MUs with 200 DR, 400 DR and 600 DR (1 DR = 1 MU/min).

In Figure 3, the normalized CTF graphs, called hereafter CTFnorm graphs, for 100 cm and 115 cm source–phantom distances for 2 MUs under 200 DR, 400 DR and 600 DR irradiation conditions are demonstrated. It can be observed that from 0.1 lp/mm to 0.27 lp/mm, the CTFnorm values show a minor variation from 0% to 2.01%. However, the CTFnorm values for the 100 cm irradiation setup are 0.01% higher. For the 115 cm distance, from 0.27 lp/mm to 0.789 lp/mm, there is an increase in CTFnorm from 0.76% to 16.09%, compared with the irradiation conditions of 100 cm. This increase at 115 cm is qualitatively reflected in the corresponding aMTFs.

Figure 4 illustrates the CTFnorm graphs for 100 cm and 115 cm source–phantom distances using 100 MUs at a 200 DR, a 400 DR and a 600 DR. The CTFnorm values for 115 cm from 0.1 lp/mm to 0.27 lp/mm present a small increase of about 0–3.25% compared to the corresponding values for the 100 cm irradiation setup. Similarly, the difference from 0.27 lp/mm to 0.463 lp/mm is about 1.27–2.11%. Furthermore, the difference in favor of the 115 cm distance from 0.463 lp/mm to 0.789 lp/mm has been found to be equal to 18.56%. In each case, the CTFnorm values for the 115 cm distance are noticeably higher for all of the spatial frequencies examined. In all cases, the standard error in the CTF calculation has been reported to range from 0.5% to 11%, depending upon the MU, DR and spatial frequency [3].

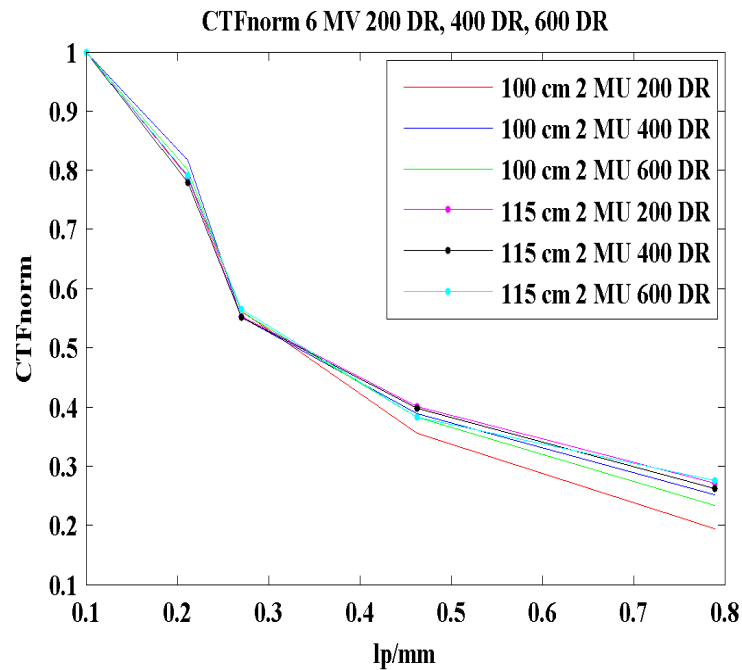


**Figure 3.** CTFnorm graphs of 100 cm using 2 MUs and 115 cm using 2 MUs with 200 DR, 400 DR and 600 DR (1 DR = 1 MU/min).

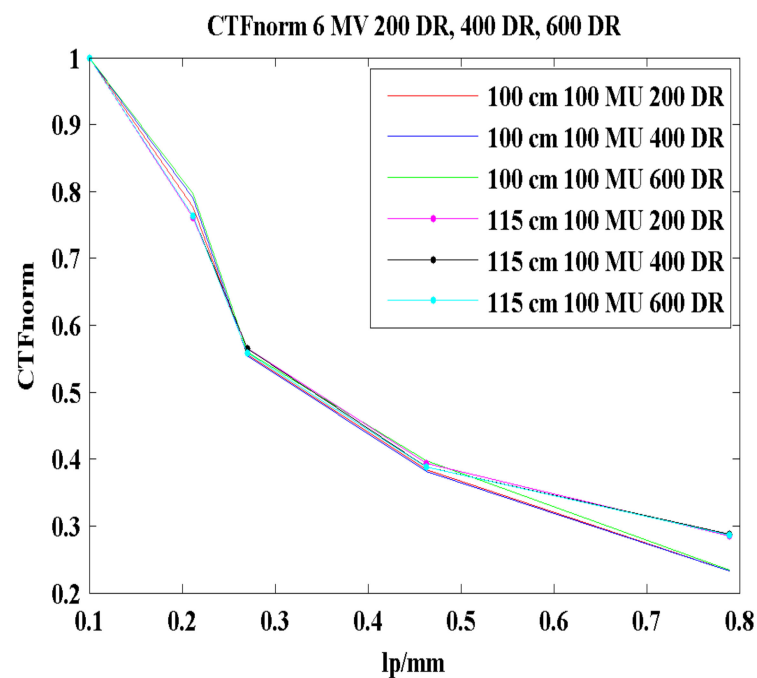


**Figure 4.** CTFnorm graphs of 100 cm using 100 MUs and 115 cm using 100 MUs with 200 DR, 400 DR and 600 DR (1 DR = 1 MU/min).

In Figure 5, the SNFR graphs, calculated by Equation (5) for 100 cm and 115 cm source-phantom distances, with 2 MUs at a 200 DR, a 400 DR and a 600 DR, are shown. From 0.1 lp/mm to 0.27 lp/mm, the difference between the SNFR curves ranges from 4.98% to 27.48%. From 0.27 lp/mm to 0.789 lp/mm, the variation stabilizes at about 7.13–8.54%. The SNFR values for the distance of 115 cm are significantly higher than those for the 100 cm distance. More specifically, at 0.1 lp/mm, the maximum differentiation of the SNFR graphs is 27.48%, with the 115 cm distance values being higher than the 100 cm values, except for

the SNFR value for 2 MUs at a 200 DR at 0.27 lp/mm. Since the SNFR is a function of the CTF, in the numerator, and the NPS, calculated by Equation (4), in the denominator, the increased numbers at 115 cm follow the corresponding CTF increase shown in Figures 3 and 4. In Figure 6, the IC (f) graphs for 100 cm and 115 cm source–phantom distances with 2 MUs at a 200 DR, a 400 DR and a 600 DR are presented. Using IC (f), or the IC before the integration, shown in Equation (6), over the frequency range was considered more practical to present a metric that helped comparisons with the SNFR. From 0.1 lp/mm to 0.27 lp/mm, the IC values show a small variation of about 0.35–0.58%. From 0.27 lp/mm to 0.789 lp/mm, the variation is about 1.26–1.41%. The IC values for the 115 cm distance are higher than those for the 100 cm distance, except for the IC value at 0.27 lp/mm for 2 MUs at a 200 DR. The increased IC (f) values are due to the corresponding increase in the aMTF shown in Figures 1 and 2.

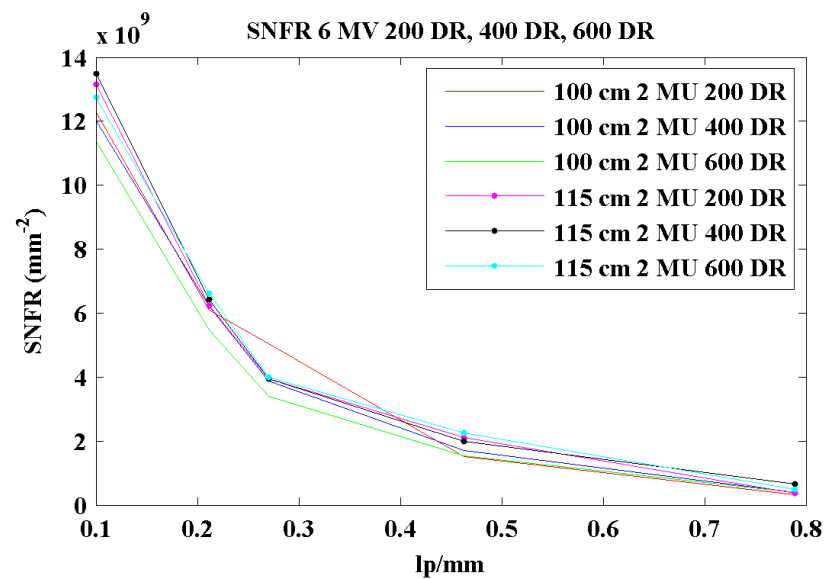


Figure 5. SNFR graphs of 100 cm using 2 MUs and 115 cm using 2 MUs with 200 DR, 400 DR and 600 DR (1 DR = 1 MU/min).

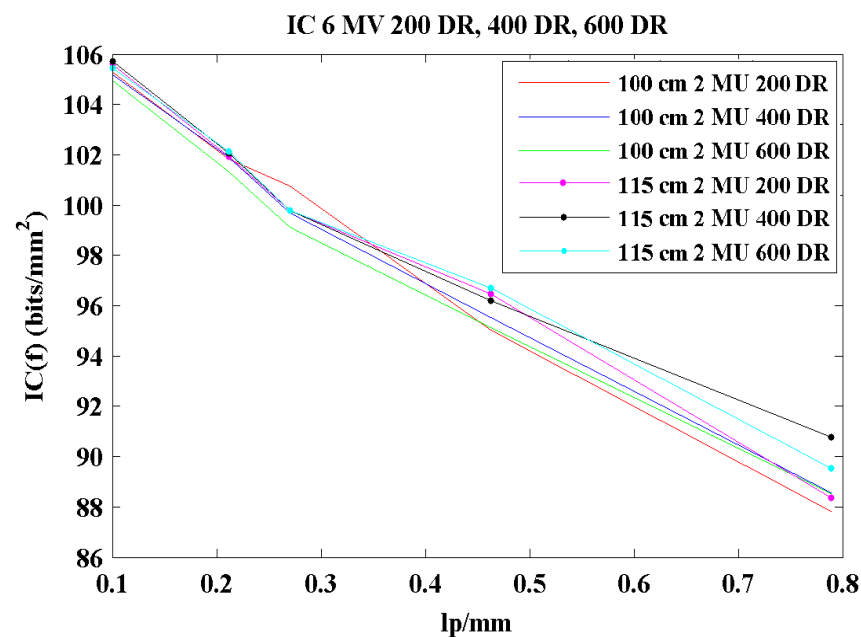
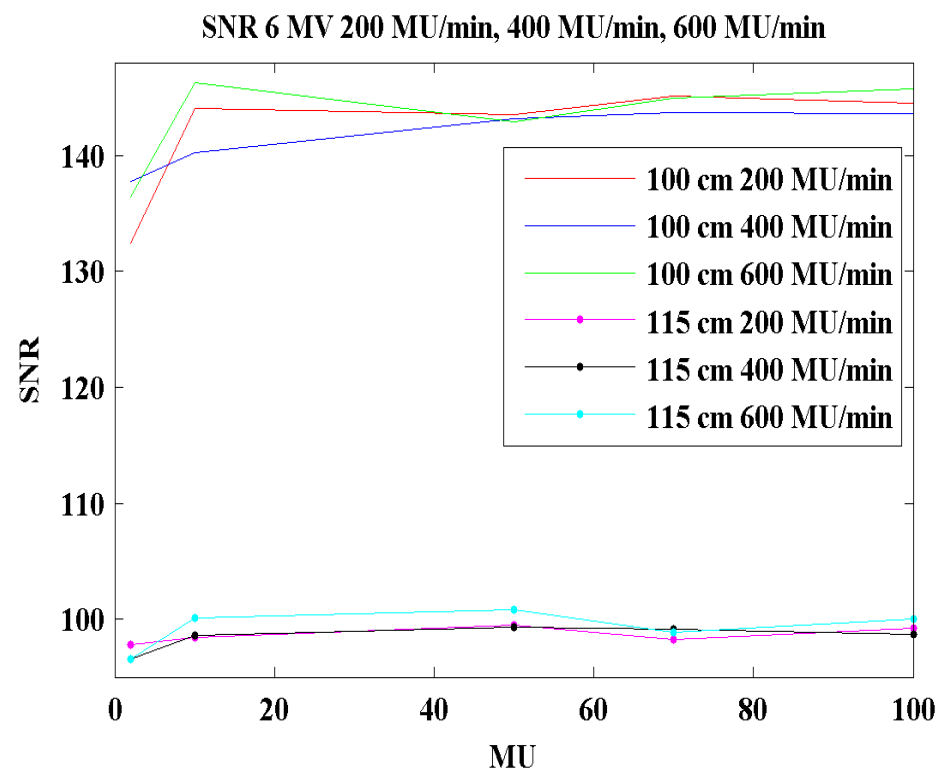


Figure 6. IC (f) graphs of 100 cm using 2 MUs and 115 cm using 2 MUs with 200 DR, 400 DR and 600 DR (1 DR = 1 MU/min).



In Figure 7, the SNR graphs, calculated by Equation (3), for 100 cm and 115 cm source–phantom distances with 2 MUs and 100 MUs at a 200 DR, a 400 DR and a 600 DR are shown. There is a noticeable differentiation of about 27.50% between the corresponding SNR values, where the SNR for 100 cm is higher. Upon inspecting Equation (3), it is seen that the SNR is proportional to the mean pixel value, corresponding to the signal, and inversely proportional to the standard deviation, expressing noise. The higher SNR at 100 cm irradiation with respect to 115 cm irradiation may be attributed to the combined effect of the signal and noise in the detector response. Considering the fact that the LINAC-to-EPID distance is the same, the corresponding difference in the SNR shown in Figure 7 may be attributed to the different spatial contributions of scatter radiation due to the closer distance of the phantom to the EPID in the 115 cm setup. The scatter spread toward the EPID under 100 cm irradiation conditions is larger, meaning that more X-rays are propagating toward the EPID periphery. The QC-3V phantom is placed at an angle [3], meaning that the part of the area of air where the SNR was calculated is toward the EPID periphery. Under the 100 cm irradiation conditions, it was exposed to primary radiation and scatter from the phantom. This scatter was larger under the 100 cm conditions than under the 115 cm conditions. Therefore, the radiation incident at the region of air where the SNR is measured was higher at 100 cm than at 115 cm. The higher radiation produces higher signal values and better noise statistics, that is less noise. Both of them yield a higher SNR value at 100 cm than at 115 cm from the LINAC head, as shown in Figure 7. The EPID signal and noise values are finally affected by the software algorithms imposed on the image before its final presentation [3].



**Figure 7.** SNR graphs of 100 cm and 115 cm with 200 DR, 400 DR and 600 DR (1 DR = 1 MU/min).

In Table 1a,b and Table 2a,b, the summation of the SNFR over spatial frequencies, called hereafter the ISNFR, and the IC calculated by Equation (6) are shown. The ISNFR as a single parameter allows for a direct comparison with the IIC. It can be shown from the tables that neither the ISNFR nor the IIC significantly vary with respect to the MU and DR [3,23,24]. In addition, both values are higher under 115 cm exposure conditions. The relative average increase in the ISNFR from 110 cm to 115 cm for all MUs and DRs is 12.5%, with a minimum value equal to 5% and a maximum of 21%. The corresponding



relative increase values for the IC parameter are a 1.1% average, a 0.01% minimum and a 2% maximum. These data imply that the ISNFR may be a more appropriate parameter for detecting changes in the performance of a LINAC.

**Table 1.** (a) Tabulated ISNFR data for 100 cm source–phantom distance with 200 DR, 400 DR and 600 DR (1 DR = 1 MU/min). (b) Tabulated ISNFR data for 115 cm source–phantom distance with 200 DR, 400 DR and 600 DR (1 DR = 1 MU/min).

100 cm Source–Phantom Distance															
	200 DR					400 DR					600 DR				
MU	2	10	50	70	100	2	10	50	70	100	2	10	50	70	100
ISNFR ( $\times 10^9$ ) mm <sup>−2</sup>	2.49	2.64	2.64	2.66	2.63	2.48	2.74	2.59	2.48	2.56	2.28	2.60	2.51	2.44	2.61
115 cm Source–Phantom Distance															
	200 DR					400 DR					600 DR				
MU	2	10	50	70	100	2	10	50	70	100	2	10	50	70	100
ISNFR ( $\times 10^9$ ) mm <sup>−2</sup>	2.67	2.82	2.82	2.90	2.91	2.79	2.88	2.89	2.89	2.98	2.74	2.96	3.02	2.95	2.86

**Table 2.** (a) Tabulated IIC data for 100 cm source–phantom distance with 200 DR, 400 DR and 600 DR (1 DR = 1 MU/min). (b) Tabulated IIC data for 115 cm source–phantom distance with 200 DR, 400 DR and 600 DR (1 DR = 1 MU/min).

100 cm Source–Phantom Distance															
	200 DR					400 DR					600 DR				
MU	2	10	50	70	100	2	10	50	70	100	2	10	50	70	100
IIC (bits/mm <sup>2</sup> )	71.98	72.34	72.30	72.65	72.27	72.25	72.98	73.09	72.28	73.08	72.05	72.82	72.15	72.19	72.72
115 cm Source–Phantom Distance															
	200 DR					400 DR					600 DR				
MU	2	10	50	70	100	2	10	50	70	100	2	10	50	70	100
IIC (bits/mm <sup>2</sup> )	72.43	73.46	73.15	73.16	73.59	73.15	73.31	73.15	73.31	74.09	72.85	73.52	73.59	73.24	73.16

#### 4. Discussion

Portal images are formed through photon beam projection on a detector, which detects a photon flux consisting of (a) primary radiation in the form of a diverging beam that attenuates according to the inverse square law and causes magnification of the imaged objects, and (b) scattered radiation originating from the phantom, which is scattered at relatively small angles.

The parameters of the SNFR and IC, defined on the basis of the aMTF and CTF, decrease with spatial frequency, although at a different rate, as can be observed from Figures 1–4. The shape of these variations is determined by two factors: (i) the relation between the signal (as expressed through the aMTF and CTF) and the noise (NPS) in the spatial frequency domain (see Equations (5) and (6)), and (ii) the mathematical relationship that defines the IC and SNFR. As has been previously mentioned [25], the MTF, and similarly the CTF, decreases with frequency faster than the NPS, and this affects the shapes of the SNFR and IC curves in the frequency space. On the other hand, the IC is defined by means of a logarithm, which compresses the range of available numerical values. For this reason, the IC appears to decay more slowly with frequency compared to the SNFR. IC has been defined as a measure of information, which is more specifically expressed by the signal corrupted by noise [26], in the context of mathematical information theory. Its use in medical imaging serves as a measure of comparison between imaging systems and is usually expressed as a single index (integrated over the frequency spectrum). In each case, the values of the IIC and ISNFR, as shown in Table 1a,b and Table 2a,b, were higher at the 115 cm irradiation distance, while the corresponding IC (f) and SNFR values were found to

decrease with spatial frequency. The latter behavior can be attributed to the changes in the CTF and MTF.

The corresponding decrease in the CTF and MTF with spatial frequency depends on various factors, including radiation fluence, source size, X-ray scattering, detector properties such as phosphor thickness, light scattering within phosphor mass, the type of optical sensor and pixel size, as well as image magnification, which is of interest in our case.

In the experimental setup presented, the properties of the detector do not affect the comparison of the aMTF and CTF results, since in both cases (100 and 115 cm) the detector is the same (flat panel imager with Gd2O2S:Tb phosphor). The same holds for the source dimensions.

However, this behavior could be attributed to two factors: (i) the effect of Compton scattering, and (ii) magnification. In radiation therapy energies (in the range of a few or several MeVs), the scattered photons are oriented within low-angle directions. That is, they impinge on the detector within a spread width that increases as a function of the phantom–detector distance. In the case of the short source–phantom distance (100 cm), the phantom–detector distance increases, and this has a similar effect on the spread width, which in turn degrades spatial resolution and the MTF. The second factor that affects parameters expressing spatial resolution is magnification. This effect is more significant in the case of 100 cm (phantom–detector distance equal to 60 cm vs. 45 cm). Magnification increases the penumbra, i.e., the geometric unsharpness around imaged structures, which in turn degrades spatial resolution and decreases the MTF at 100 cm.

In the case of the zero-frequency SNR, shown in Figure 4, the source–phantom distance of 100 cm produces higher values, apparently due to the inverse square law (i.e., radiation intensity is proportional to the inverse of the square of the distance), which corresponds to higher  $\mu_{ROI}$  values at lower distances (see relation (3)) (recall that if Poisson statistics are assumed, the denominator of the SNR is equal to the square root of  $\mu$  and therefore increases at a slower rate than  $\mu_{ROI}$ ).

Based on the previous discussion, we can state that increasing the source–phantom distance from 100 cm to 115 cm results in image quality improvement at multiple levels. Image quality enhances across nearly all spatial frequencies, as evidenced by the aMTF, CTFnorm, SNFR and IC values. Furthermore, increasing the MUs to the maximum (100 MU) further ameliorates image quality.

The results of our study provide a solid methodology relying on typical quality control measurements for calculating multivariate parameters like the SNFR and IC in order to check the EPID performance of a LINAC in terms of the signal-to-noise ratio in the spatial frequency domain. These values can be used for checking deviations in EPID performance, which is also useful in the application of EPID dosimetry [27]. In addition, our results with respect to distance may be of importance for better realization of three-dimensional organ images when a two-dimensional EPID image is acquired.

## 5. Conclusions

In this study, we investigated the influence of source–phantom distance and monitor unit (MU) settings as LINAC irradiation parameters on the image quality of electronic portal imaging systems (EPIDs) using quantitative quality metrics. Image quality was evaluated using the QC-3V EPID phantom, showing its successful applicability in quality control procedures. In addition, metrics analyzed in the spatial domain, such as the SNR, and spatial frequency-dependent image quality metrics associated with the signal and noise transfer characteristics of detectors can be determined. In this study, we examined parameters such as the aMTF, CTFnorm, SNFR and IC. The SNFR proves to be valuable for assessing the overall system output performance and can be conveniently evaluated in a clinical setting. Additionally, IC values, either integrated or as a function of frequency (IC (f)), are useful metrics for estimating both image quality and the performance of the EPID. The aforementioned metrics can be regularly employed for evaluating the performance of LINAC and EPID systems, complementing existing image quality procedures. They can aid

in optimizing various settings during portal imaging procedures and checking deviations in EPID performance. In addition, our results with respect to distance may be of importance in the realization of three-dimensional organ images when a two-dimensional EPID image is acquired. Further work may incorporate our findings in EPID dosimetry applications.

**Author Contributions:** Conceptualization, M.K.T., N.K. and I.S.K.; methodology, M.K.T. and I.S.K.; software, M.K.T.; validation, C.M., N.K. and I.V.; formal analysis, I.S.K.; investigation, I.S.K.; resources, G.F., V.P., A.A., G.K. and A.E.; data curation, M.K.T.; writing—original Draft preparation, M.K.T., I.S.K. and N.K.; writing—review and editing, M.K.T., I.V., C.M., V.P., A.A., N.K. and I.S.K.; visualization, M.K.T.; supervision, N.K. and I.S.K.; project administration, N.K. and I.S.K. All authors have read and agreed to the published version of the manuscript.

**Funding:** This research received no external funding.

**Institutional Review Board Statement:** Not applicable.

**Informed Consent Statement:** Not applicable.

**Data Availability Statement:** The original contributions presented in the study are included in the article, further inquiries can be directed to the corresponding author.

**Conflicts of Interest:** Anastasios Episkopakis is an employee of Elekta.

## References

1. Son, S.-Y.; Choi, K.-W.; Kim, J.-M.; Jeong, H.-W.; Kwon, K.-T.; Cho, J.-H.; Lee, J.-H.; Jung, J.-Y.; Kim, K.-W.; Lee, Y.-A.; et al. Evaluation of Image Quality for Various Electronic Portal Imaging Devices in Radiation Therapy. *J. Radiol. Sci. Technol.* **2015**, *38*, 451–461. [CrossRef]
2. Klein, E.E.; Hanley, J.; Bayouth, J.; Yin, F.; Simon, W.; DRESSER, S.; Serago, C.; Aguirre, F.; Ma, L.; Arjomandy, B.; et al. Task Group 142 report: Quality Assurance of Medical Accelerators. *Med. Phys.* **2009**, *36*, 4197–4212. [CrossRef] [PubMed]
3. Tzomakas, M.K.; Peppas, V.; Alexiou, A.; Karakatsanis, G.; Episkopakis, A.; Michail, C.; Valais, I.; Fountos, G.; Kalyvas, N.; Kandarakis, I.S. A phantom based evaluation of the clinical imaging performance of electronic portal imaging devices. *Heliyon* **2023**, *9*, e21116. [CrossRef] [PubMed]
4. Das, I.J.; Cao, M.; Cheng, C.; Mistic, V.; Scheuring, K.; Schüle, E.; Johnstone, P.A. A quality assurance phantom for electronic portal imaging devices. *J. Appl. Clin. Med. Phys.* **2011**, *12*, 391–403. [CrossRef]
5. Borasi, G.; Nitrosi, A.; Ferrari, P.; Tassoni, D. On site evaluation of three flat panel detectors for digital radiography. *Med. Phys.* **2003**, *30*, 1719–1731. [CrossRef]
6. Cremers, F.; Frenzel, T.; Kausch, C.; Albers, D.; Schönborn, T.; Schmidt, R. Performance of electronic portal imaging devices (EPIDs) used in radiotherapy: Image quality and dose measurements. *Med. Phys.* **2004**, *31*, 985–996. [CrossRef]
7. Munro, P.; Bouius, D.C. X-ray quantum limited portal imaging using amorphous silicon flat-panel arrays. *Med. Phys.* **1998**, *25*, 689–702. [CrossRef]
8. Gopal, A.; Samant, S.S. Use of a line-pair resolution phantom for comprehensive quality assurance of electronic portal imaging devices based on fundamental imaging metrics. *Med. Phys.* **2009**, *36*, 2006–2015. [CrossRef]
9. Kanamori, H.; Matsumoto, M. The information spectrum as a measure of radiographic image quality and system performance. *Phys. Med. Biol.* **1984**, *29*, 303–313. [CrossRef]
10. Michail, C.M.; Kalyvas, N.E.; Valais, I.G.; Fudos, I.P.; Fountos, G.P.; Dimitropoulos, N.; Koulouras, G.; Kandris, D.; Samarakou, M.; Kandarakis, I.S. Figure of Image Quality and Information Capacity in Digital Mammography. *BioMed Res. Int.* **2014**, *2014*, 634856. [CrossRef]
11. Shannon, C.E. A Mathematical Theory of Communication. *Bell. Syst. Tech. J.* **1948**, *27*, 379–423. [CrossRef]
12. Michail, C.; Karpetsas, G.; Kalyvas, N.; Valais, I.; Kandarakis, I.; Agavanakis, K.; Panayiotakis, G.; Fountos, G. Information Capacity of Positron Emission Tomography Scanners. *Crystals* **2018**, *8*, 459. [CrossRef]
13. SeeDOS Ltd. *The Quality Control Phantom QC-3*. 2008. Available online: [http://www.seedos.co.uk/qc3\\_phantom.htm](http://www.seedos.co.uk/qc3_phantom.htm) (accessed on 14 December 2022).
14. Michail, C.; Spyropoulou, V.; Kalyvas, N.; Valais, I.; Dimitropoulos, N.; Fountos, G.; Kandarakis, I.; Panayiotakis, G. The influence of software filtering in digital mammography image quality. *J. Instrum.* **2009**, *4*, P05018. [CrossRef]
15. Haus, A.G. *The Physics of Medical Imaging: Recording System, Measurements and Techniques*; Wiley: New York, NY, USA, 1979.
16. Nill, N.B. Conversion Between Sine Wave and Square Wave Spatial Frequency Response of an Imaging System, MITRE. 2001. Available online: <https://apps.dtic.mil/sti/citations/ADA460454> (accessed on 7 March 2023).
17. Boreman, G.D. *Modulation Transfer Function in Optical and Electro-Optical Systems*; SPIE: Bellingham, WA, USA, 2001. [CrossRef]
18. Boone, J.M.; Yu, T.; Seibert, J.A. Sinusoidal modulation analysis for optical system MTF measurements. *Med. Phys.* **1996**, *23*, 1955–1963. [CrossRef] [PubMed]
19. Podgorsak, E.B. *Radiation Oncology Physics: A Handbook for Teachers And Students*; IAEA: Vienna, Austria, 2005.

20. De Moura, F.M.G. Amorphous Silicon Detector Panel Damage: Correlating Physical Parameters to Clinical Usability. Master's Thesis, Universidade de Lisboa, Lisbon, Portugal, 2008. Available online: <https://repositorio.ul.pt/handle/10451/1277?locale=en> (accessed on 7 March 2023).
21. Kilic, K.; Erbas, G.; Guryildirim, M.; Konus, O.L.; Arac, M.; Ilgit, E.; Isik, S. Quantitative and Qualitative Comparison of Standard-Dose and Low-Dose Pediatric Head Computed Tomography: A Retrospective Study Assessing the Effect of Adaptive Statistical Iterative Reconstruction. *J. Comput. Assist. Tomogr.* **2013**, *37*, 377–381. [[CrossRef](#)]
22. Williams, M.B.; Mangiafico, P.A.; Simoni, P.U. Noise power spectra of images from digital mammography detectors. *Med. Phys.* **1999**, *26*, 1279–1293. [[CrossRef](#)]
23. McDermott, L.N.; Louwe, R.J.W.; Sonke, J.-J.; van Herk, M.B.; Mijnheer, B.J. Dose-response and ghosting effects of an amorphous silicon electronic portal imaging device. *Med. Phys.* **2003**, *31*, 285–295. [[CrossRef](#)]
24. Liu, J.; Xu, Y.; Teymurazyan, A.; Papandreou, Z.; Pang, G. Development of a novel high quantum efficiency MV x-ray detector for image-guided radiotherapy: A feasibility study. *Med. Phys.* **2019**, *47*, 152–163. [[CrossRef](#)]
25. Nishikawa, R.M.; Yaffe, M.J. Model of the spatial-frequency-dependent detective quantum efficiency of phosphor screens. *Med. Phys.* **1990**, *17*, 894–904. [[CrossRef](#)]
26. Wagner, R.F.; Brown, D.G.; Pastel, M.S. Application of information theory to the assessment of computed tomography. *Med. Phys.* **1979**, *6*, 83–94. [[CrossRef](#)]
27. Olaciregui-Ruiz, I.; Beddar, S.; Greer, P.; Jornet, N.; McCurdy, B.; Paiva-Fonseca, G.; Mijnheer, B.; Verhaegen, F. In vivo dosimetry in external beam photon radiotherapy: Requirements and future directions for research, development, and clinical practice. *Phys. Imaging Radiat. Oncol.* **2020**, *15*, 108–116. [[CrossRef](#)]

**Disclaimer/Publisher's Note:** The statements, opinions and data contained in all publications are solely those of the individual author(s) and contributor(s) and not of MDPI and/or the editor(s). MDPI and/or the editor(s) disclaim responsibility for any injury to people or property resulting from any ideas, methods, instructions or products referred to in the content.